Heliyon 9 (2023) e22403

Contents lists available at ScienceDirect

Heliyon

journal homepage: www.cell.com/heliyon

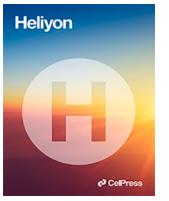

Enhanced electrocatalytic properties in dye-sensitized solar cell via Pt/SBA-15 composite with optimized Pt constituent

Ding Nan, Hongzhi Fan, Altan Bolag *, Wenhui Liu, Tana Bao

Inner Mongolia Key Laboratory for Physics and Chemistry of Functional Materials, Engineering Research Center of New Energy Storage Materials at Universities of Inner Mongolia Autonomous Region, College of Physics and Electronic Information, Inner Mongolia Normal University, No 81 Zhaowuda Road, Saihan district, Hohhot, 010022, China

ARTICLE INFO

Keywords:
Dye-sensitized solar cells
Counter electrode
Molecular sieves
SBA-15
Electrocatalytic property

ABSTRACT

The Low utilization and high cost of platinum counter electrode (CE) in the application of dye-sensitized solar cells has limited its large-scale manufacturing in the industry. Herein, a facile pyrolysis combination of Pt and SBA-15 molecular sieve (MS) formed 1.6–1.9 times higher amount and 2–3 times reduced dimension of Pt distributed within porous structure of SBA-15. The composite CE with 20 % of SBA-15 exhibited an enhanced power conversion efficiency of 9.31 %, exceeding that of absolute Pt CE (7.57 %). This superior performance owed to the promoted oxidation-reduction rate of I_3^-/I^- pairs at the CE interface and the increased conductivity of CE materials attributed from well distributed Pt particles. This work has demonstrated the significance of utilizing porous molecular sieves for dispersing catalytic sites when designing a novel type of counter electrode and their application in DSSCs.

1. Introduction

Because of their superior indoor low light performance and facile fabrication than a-Si and organic photovoltaic (OPV) solar cells [1], dye-sensitized solar cells (DSSCs) have been known as one of the increasingly intriguing solar power system for a variety of indoors techniques, counting the Internet of Things and fifth-generation wireless communication [2–5]. A typical DSSC is comprised of a semi-conductive metal oxide photoanode (PA), a light collection ssensitizer, an electrolytic redox pair and a catalytic counter electrode (CE). The working principle of DSSC is as follows. Solar energy irradiation causes an electron to be stimulated from the ground state to the excited state of the dye molecule, and then the electron injects into the conduction band of PA. The external load conducts the electron from the PA to the CE electrode, where it participates in the process of regenerating electrolyte components. Finally, the oxidized dye obtains an electron from the electrolyte, completing the cycle. Platinum is well-known for being one of the best CE materials due to its high conductivity and catalytic capability, which can efficiently collect electrons from the external circuit to the cell and catalyze the reduction-oxidation process between the electrolyte components [6]. However, absolute Pt as of precious metal is unsuitable for low-cost and large-scale DSSC production in long term. Thus, it has been well-concerned research direction to develop CE materials consisted with less or absence of Pt for achieving an equivalent DSSC performance. Alternative CEs such as conductive polymers [7] or various of oxides [8,9], sulfides [10,11], nitrides [12] and metal alloys [13] have been explored and some of them performed remarkable properties as CEs especially in the presence of Co- and Cu-based redox couples rather than iodine electrolyte. While the mentioned polymers and inorganic compounds usually required complex synthetic process as well as sophisticated

* Corresponding author.
E-mail address: altan.bolag@imnu.edu.cn (A. Bolag).

https://doi.org/10.1016/j.heliyon.2023.e22403
Received 31 July 2023; Received in revised form 1 November 2023; Accepted 10 November 2023
Available online 14 November 2023

deposition method on FTO substrate. Another optional CE based on carbon material owns advantages of low-cost, extensive resource and high conductivity [14,15]. Nevertheless, carbon materials do not possess the same catalytic properties as Pt, and their adhesion to fluorine-doped tin oxide (FTO) substrates is weak. This results in elevated series resistance, and ultimately reduces power conversion efficiency (PCE), making it challenging to produce large area modules.

The structural defects of carbon-based materials play an important role in regulating their catalytic activity in terms of changing the electron distribution of carbon materials, which is highly depended on the developed pores, large surface area, and unique advantages of large micro-mesoporous volume [16–19]. Porous structure also helps to disperse expensive catalytic precious metals for increasing the surface volume ratio of the catalytic metals and thus make the best of the metal within catalytic process. Hence, dual effects of catalysis are realizable by means of compositing porous materials with metal catalyst. As mesoporous aluminosilicates, molecular sieves (MS) have hydrothermal/thermal and mechanical stability, a large surface area, a high pore volume, and an open pore structure, and therefore are widely used in drug delivery, sensor, absorbent, separation, and catalysis [20–22]. To the best of one's knowledge, molecular sieves have not ever been introduced as catalyst support of CEs in DSSCs. In this study, a molecular sieve SBA-15 with a greater porosity than carbon was coupled with Pt using a simple pyrolysis method to produce more efficient CEs for DSSCs. The morphology of the CEs was characterized using XRD and SEM, while the transmissivity was examined using UV–vis spectroscopy. Electrocatalytic, Tafel, and electrochemical impedance spectra measurements were conducted, and the photovoltaic performance of the assembled cells was systematically investigated. In the presence of SBA-15 with a large specific surface area, fine and larger loading of Pt particles realized on FTO substrate by the pyrolytic reaction. The application of SBA-15 with Pt yielded successful catalytic properties, revealing remarkable DSSC efficiencies through the synergistic effect of the two materials. Pt combined with 20 % of SBA-15 produced a solar cell with a PCE of 9.31 %, which is 23 % higher than that of a platinum-based DSSC under the same conditions. The application of SBA-15 composite is not only a cost-effective solution for reducing Pt consume, but also can improve the utilization of CE materials.

2. Experimental sections

2.1. Materials, instruments and methods

The reagents and solvents used in this work were commercially viable from Sigma-Aldrich, Aladdin Scientific Corp and Macklin Incorporated. The molecular sieve SBA-15 was viable from Nanjing XFNANO Materials Tech Co., Ltd. Transmittance study of the composite films was performed via Perkin–Elmer Lambda 35 UV–visible spectrometer in order to compare the content of Pt particles in the composite films. X-ray diffraction (XRD) characterization is completed for purpose of analyzing their phase identification, sample purity and crystallite size. The phase identification was performed using X-ray diffraction (XRD, Cu Kα radiation, Philips PW1830). The 2θ scans were taken between 20° and 80° with steps of 0.05°, with 2 s counting time per angular value. Scanning electron microscopy (SEM) method was performed to further verify the nanocrystalline morphology and the variation of Pt grain size in the composite materials, using a field-emission scanning electron microscope (SEM, Hitachi SU-8010). Electrocatalytic properties were tested by a Zannium electrochemical workstation (Zahner, Germany) in a three-electrode system with a Pt wire and saturated calomel electrodes (SCE) as the counter electrode and the reference electrodes under an argon atmosphere. The electrolyte used in CV system is composed of I_3^-/I^- redox system prepared with 1 mM iodine, 10 mM lithium iodide, and 100 mM lithium perchlorate in acetonitrile solution.

2.2. Preparation of composite counter electrode

General procedure for preparing Pt/SBA15 composite counter electrodes: Glass substrates coated with fluorine-doped tin oxide (FTO) were rinsed in an ultrasonic bath with detergent solution, distilled H_2O, and EtOH, then cleaned with H_2O and EtOH and dried with nitrogen flow subsequently. Different proportions (0 %, 10 %, 20 % and 30 %) of SBA15 molecular sieves with the same quantity (212 mg) of chloroplatinic acid hexahydrate ($H_2PtCl_6{\cdot}6H_2O$) were adequately mixed and sonicated in iso-propyl alcohol solvent, labeled as Pt, Pt/SBA1, Pt/SBA2 and Pt/SBA3, respectively. The prepared mixture was deposited over FTO glass via drop-cast method, followed by 400 °C temperature sintering in a muffle furnace for 30 min.

2.3. Fabrication of DSSC

Nanocrystalline film consisted with TiO_2 paste of 20 nm nanoparticles was fabricated on FTO substrates via screen-printing technique. The PA was gradually sinter to 500 °C and hold for 15 min within a box furnace, followed by natural cooling. The prepared TiO_2 electrode was further treated with a $TiCl_4$ aqueous solution of 40 mM at 70 °C for 30 min, then rinsed in order of H_2O and EtOH, and sintered under 450 °C for 30 min followed by natural cooling. Prior to a sensitization with N719 dye solution of 0.3 mM for 24 h, the photoanode was initiated at 80 °C for 30 min. A sandwich structure of DSSC was assembled with the sensitized PA, CE as well as electrolyte solution according to our previous work [23].

Fabrication of symmetric dummy DSSC: In order to test electrochemical impedance spectroscopy and Tafel curve, CE with and without holes were assembled into a dummy cell through encapsulation and electrolyte injection. The hole was sealed using UV-curable adhesive and glass slide, subsequently.

2.4. Photovoltaic characterizations

In order to remove light diffusion on the apparent surface area (ca. 0.36 cm^2) of the DSSC, a lightproof mask with aperture area of 0.03 cm^2 was applied before irradiation of a simulated AM 1.5G sunlight (XES-70S1, SAN-EI Electric, Japan). DSSC photovoltaic performance was investigated via photocurrent–voltage (*J–V*) measurement.

3. Results and discussion

3.1. Morphology and micro-structure of the prepared Pt/SBA15 composites

The crystal structures of Pt/SBA-15 composite films were investigated by XRD patterns, as displayed in Fig. 1. All the films showed the diffraction peaks of FTO layer at 27°, 38°, 52° and 62°. The obvious diffraction peaks observed at 39.6°, 46.4° and 67.7°, were assigned to the (111), (200) and (220) planes of Pt, respectively. As the amount of SBA-15 increased successively from Pt to Pt/SBA3, the characteristic Pt peaks slightly shifted towards small angle and the intensity was weakened as well, indicating that the lattice constant became larger and the grain size of Pt decreased. When X-rays are incident on small crystals, the diffraction lines become diffuse and broadened, and the smaller the grain size of the crystal, the greater the broadening of the X-ray diffraction bands. The smaller Pt particles formed within SBA-15 composite CE holding larger specific surface area of contact with the electrolyte components are able to provide more catalytic active sites, which is desirable for enhancing DSSC performance. Small-angle XRD was applied to confirm the presence of SBA-15, however, due to the low contents of SBA-15 in the composite, the diffraction peak at 0.7°–0.8° corresponded to (100) plane of SBA-15 was not detected.

Fig. 2 depicts the shape and microstructure of Pt and composite films on an FTO glass substrate. As in Fig. 2a, Pt particles with diameters of 20–25 nm were homogeneously distributed on the exterior of the FTO film in the absence of SBA-15. When combined with SBA-15, the Pt particle generated by pyrolysis process firmly adsorbed both outside and inside the SBA-15 through-hole structure at a 2–3 times smaller size of 8–10 nm (Fig. 2b–d), confirming the XRD results. The undersized Pt particles aid in the formation of many more catalytic sites for reach high mass activities in catalysis [24].

The transmission curves of the produced Pt/SBA-15 electrodes in the wavelength range of 300–800 nm are shown in Fig. 3. The pure SBA-15 film had a high transmittance of 95–98 %. As the portion of SBA-15 in the Pt/SBA-15 composites increased, the film transmittance reduced from 71 % to 57 % and 52 %. The Pt content in the composite films can be roughly estimated [25,26] according to logarithmic relationship of absorbance and transmittance, and the Bouguer–Lambert–Beer law hereunder [27], where *A* represents the absorbance, *T* is the transmittance, *K* is the molar absorption coefficient, *b* is the optical path length and *c* represents the concentration of Pt.

$$A = -\log(T) = Kbc \tag{1}$$

The proportion of Pt contained in the films of Pt, Pt/SBA2 and Pt/SBA3 can be estimated as 0.1487: 0.2441: 0.284, respectively, indicating that the Pt content associated on the electrode has increased by a factor of 1.6 and 1.9, based on the molecular sieves amount increasement.

3.2. Photovoltaic performance of the DSSC based on the Pt/SBA-15 composite CEs

The *J-V* characterization curves and photovoltaic performance parameters of DSSC assembled with the Pt/SBA-15 composite CEs are displayed in Fig. 4 and Table 1 severally. The DSSC based on reference platinum CE exhibited a power conversion efficiency of 7.57 % with a short-circuit current density J_{sc} of 18.32 mA/cm^2, open-circuit voltage V_{oc} of 0.63 V and fill factor *FF* of 65.73. As the SBA-15 amount increased in the composite CEs, the V_{oc} shifted slightly whereas the *FF* value trend towards raising at Pt/SBA1 firstly and reduction at Pt/SBA2 and Pt/SBA3 counter electrode. The reason is that the SBA-15 augmentation enhanced the Pt constituent,

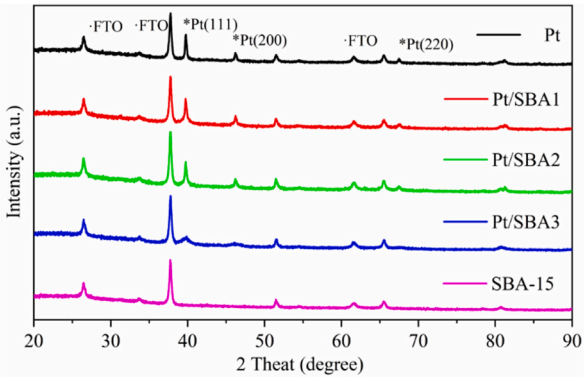

Fig. 1. XRD diffraction patterns of Pt, Pt/SBA-15 composites and SBA-15.

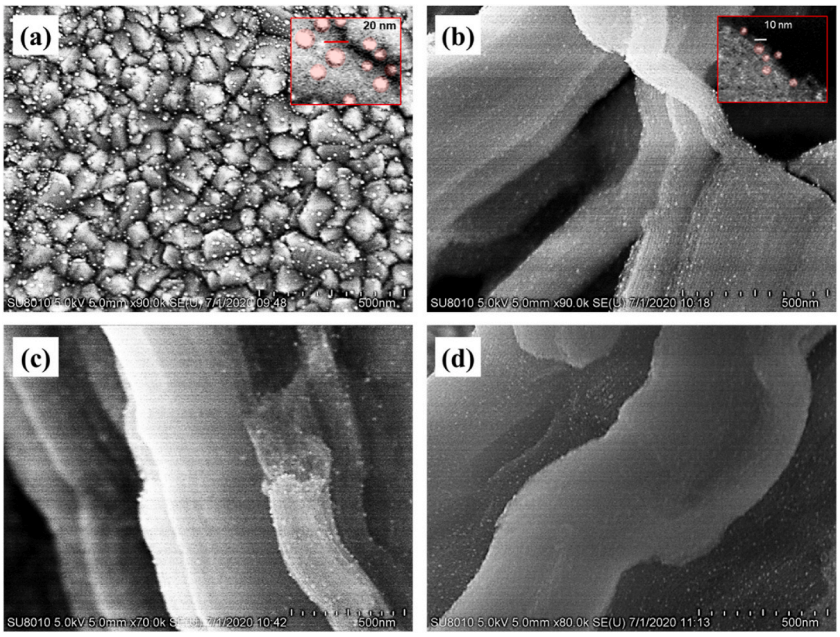

Fig. 2. SEM image of Pt and Pt/SBA-15 composite CEs, (a) Pt, (b) Pt/SBA1, (c) Pt/SBA2, (d) Pt/SBA3.

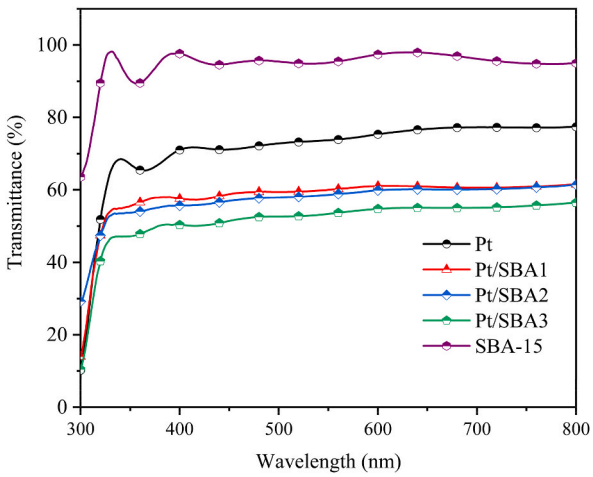

Fig. 3. Transmission curve of Pt, Pt/SBA-15 composites and SBA-15.

resulting in greater conductivity of Pt/SBA1, whereas an excess of molecular sieves presumably caused less conductive Pt/SBA2 and Pt/SBA3, since the DSSC based on SBA-15 only showed a fill factor of merely 37.47. The J_{sc} of the cells with composite CEs gradually enhanced from 18.32 to 20.73, 22.77 and 21.54 mA/cm^2, respectively. This is probably caused by faster oxidation-reduction kinetics resulting from extended catalytic activation of smaller and surpassing amount of Pt particles in Pt/SBA-15 composite CEs, which is further discussed in the following investigation of their electrochemical properties. Three composite CEs raised the PCE by 15–23 % to 8.78, 9.31 and 8.52 %, severally. Pt/SBA2 electrode exhibited the highest PCE of 9.31 % with J_{sc} of 22.77 mA/cm^2, V_{oc} of 0.64 V and *FF* of 63.65.

3.3. Electrochemical properties of the Pt/SBA-15 composite CEs

Next, in the interest of illustrating catalytic activity of the composite CEs, cyclic voltammetry, electrochemical impedance spectroscopy and Tafel polarization plot were performed successively. Cyclic voltammetry (CV) is of examining the electrocatalytic activity of CE materials and diffusion of redox ion in the electrolyte by comparing the shape and position of redox current peaks. The test was a three-electrode system, in which the prepared counter electrode was used as a working electrode, a Pt wire as the auxiliary electrode,

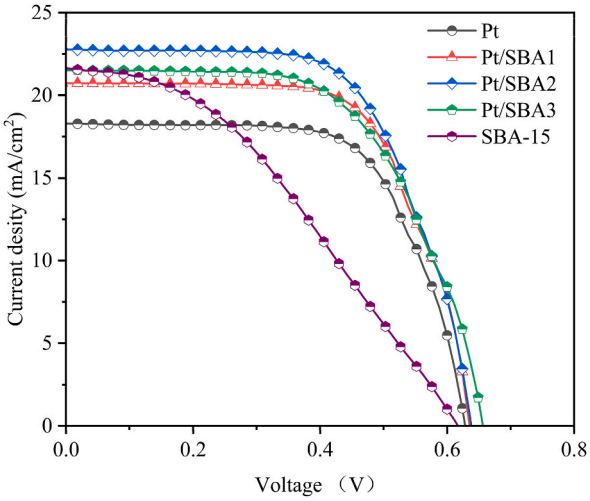

Fig. 4. *J-V* characteristic curve of the DSSCs based on Pt, Pt/SBA-15 composites and SBA-15.

Table 1
Photovoltaic performance parameters of DSSCs based on the composite CEs.

CE	V_{oc} (V)	J_{sc} (mA/cm^2)	*FF* (%)	*PCE* (%)
Pt	0.63 ± 0.01	18.38 ± 0.15	62.44 ± 3.29	7.26 ± 0.31
Pt/SBA1	0.63 ± 0.01	20.60 ± 0.61	62.48 ± 3.68	8.12 ± 0.66
Pt/SBA2	0.63 ± 0.01	21.77 ± 0.70	63.21 ± 0.52	8.68 ± 0.58
Pt/SBA3	0.65 ± 0.01	21.27 ± 0.52	59.20 ± 0.83	8.16 ± 0.41
SBA-15	0.60 ± 0.01	21.50 ± 0.49	38.04 ± 0.72	4.95 ± 0.06

and a saturated calomel electrode (SCE) as the reference electrode. The electrolyte is an acetonitrile solution of I_3^-/I^- redox pairs prepared from 1 mM iodine, 10 mM lithium iodide and 100 mM lithium perchlorate.

As shown in Fig. 5, two couples of obvious oxidation-reduction current-density peaks were presented for all the electrodes, indicating their similar catalytic behaviors. The first and second redox peaks are attributed to I_3^-/I^- and I_2/I_3^- oxidation-reduction peaks, respectively. The catalytic properties of electrode materials are mainly determined by the potential's dissimilarity between the anodic and cathodic redox peaks ($\Delta E_{pp} = |E_{red} - E_{ox}|$) and absolute value of the first reduction peak current density (J_{red}). The ΔE_{pp} value shows an inverse correlation with the oxidation-reduction rate and a smaller ΔE_{pp} indicates a faster electrochemical redox kinetics. As the amount of SBA-15 increased from Pt to Pt/SBA1 and Pt/SBA2, the Pt particles uniformly distributed inside the porous structure of SBA-15 and the diffusion route formed successfully between electrolyte and electrode, and thus Pt/SBA2 electrode showed the lowest value of E_{pp}, indicating its faster diffusion magnitude between electrolyte and electrode. The reaction rate of the catalyst for the

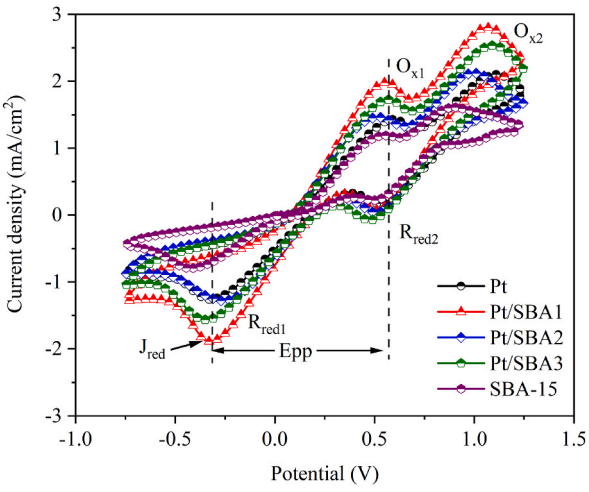

Fig. 5. Cyclic voltammetry curve of Pt, Pt/SBA-15 composites and SBA-15 electrodes.

reduction of I_3^- to I^- is affected by $|J_{red}|$. Remarkably, the $|J_{red}|$ value increases in the order of SBA-15 < Pt < Pt/SBA2 < Pt/SBA3 < Pt/SBA1, suggesting that the introduction of molecular sieves positively enhanced the reduction to the electrode. While owing a reduced $|J_{red}|$ value than Pt/SBA3 and Pt/SBA1, Pt/SBA2 has better comprehensive effect of electrocatalytic activity than other CEs due to its lower E_{pp}, as well as R_s and R_{ct} value in the following EIS measurement. It has also been reported previously that a counter electrode with a lower $|J_{red}|$ value but better EIS and Tafel properties exhibits improved photovoltaic performance [28,29].

As in Table 2, the Pt/SBA-15 composite CEs have smaller ΔE_{pp} and greater $|J_{red}|$ values than those of platinum CE, especially, Pt/SBA2 showed a ΔE_{pp} of 0.76 V, which is 0.14–0.17 V smaller than that of the other composite CEs (0.90 and 0.92 V) and the pristine Pt counter electrode (0.93 V). Interestingly, both J_{red} and ΔE_{pp} values had a tendency to boost the catalytic property firstly and then moderate according to the presented ratio of SBA-15 in composite. This is in accordance with the variation trend of the *FF* and J_{sc} values in photovoltaic performance of the corresponded solar cells.

Subsequently, interfacial electrochemical properties of DSSCs were investigated by electrochemical impedance spectroscopy EIS and Tafel polarization analysis for the symmetric dummy cells with as-prepared CEs. The fitting results of the recorded EIS spectra obtained with Z-view software were shown in Fig. 6, with the equivalent circuit depicted in the inset. The impedance of dye-sensitized solar cells (Z_{DSSC}) can be expressed as the sum of the impedance of Ohmic series resistance (R_s), the impedance of charge transfer resistance at the counter electrode (R_{ct}), the impedance of charge transfer resistance at the working electrode (Z_{we}), and the impedance of I_3^- diffusion (Z_D) [30,31]. Among them, R_s and R_{ct} values are frequently discussed since they can be seen more clearly in plots. In the Nyquist plots, the intersections of the semicircles with X-axis stands for the ohmic series resistance R_s between the substrate and the CE materials, diameter of the semicircles is directly proportional to the charge transfer resistance R_{ct} between CE and electrolyte interface. As the differences in these DSSC devices resulted from their CE, the R_{ct} values have a salient influence on electrochemical properties and photovoltaic efficiency, the smaller R_{ct} values, the superior electrocatalytic activity and faster electron transport of the CE, making for higher solar cell performance [32–35]. Pt/SBA2 CE shows the smallest R_s value of 16.25 Ω cm^2, indicating its better conductivity and thus DSSC performance. Moreover, the R_{ct} of Pt/SBA2 CE is also lower than that of Pt and other composite CE, proving its elevated electrocatalytic activity for the reduction of I_3^-. The EIS results are consistent with the results obtained from the CV tests, as well as the ones from Tafel curves in the following experiments.

The performed Tafel polarization plots of as-prepared dummy cells were shown in Fig. 7. The exchange current density (J_0) expresses inherent rates of electron transfer between electrolyte and CE electrode that can be obtained according to equation (2) hereunder, where *R* represents the universal gas molar constant, *T* is the thermodynamic temperature, *n* is the number of charges transferred at the interface of electrolyte and CE, and *F* represents the Faraday constant [36].

$$J_0 = \frac{RT}{nFR_{ct}} \tag{2}$$

J_0 is inversely related to R_{ct} in the EIS, and the order of R_{ct} calculated from the equation as follows: Pt/SBA2 < Pt < Pt/SBA1 < Pt/SBA3, which coincides with the EIS data.

$$J_{lim} = \frac{2neDCN_A}{l} \tag{3}$$

Diffusion-limited current density (J_{lim}) in the diffusion zone ($|V| > 400$ mV) of Tafel plots correlates to a diffusion coefficient of the I_3^-/I^- redox species within CE. It can be obtained from equation (3), where *e*, *D*, *C*, N_A and *l* represent the charge, diffusion coefficient of redox pairs, the triiodide concentration of the electrolyte and Avogadro's constant and diffusion length, respectively [36]. While the percentage of SBA-15 in the composite is raised from 0 to 20 %, J_{lim} value gradually lifted from 1.68 to 1.72 mA/cm^2, however, Pt/SBA3 with 30 % of SBA-15 presented a diminished J_{lim} of 1.56 mA/cm^2. It implies that sufficient routes for redox diffusion rely on the conductivity of the Pt in composite CE rather than the amount of Pt.

4. Conclusion

Taken together, for the first time, we exhibited that high porous SBA-15 produced 2–3 times smaller size and 1.6–1.9 times elevated quantity of Pt particles through via pyrolysis reaction with $H_2PtCl_6{\cdot}6H_2O$, which is capable of optimizing the catalytic properties of CEs, leading to the improved photovoltaic performance. The composite CEs presented 16 %, 23 % and 15 % enhancement to the PCE of DSSC based on N719 from 7.57 % to 8.78 %, 9.31 % and 8.52 %, severally. This research has demonstrated the significance of utilizing porous molecular sieves for dispersing catalytic sites when designing a novel type of counter electrode and their application in DSSCs. The catalytic behaviors and DSSC performance of the composite CEs also depend on the MS species, preparation methods and fine control of the proportion. Further investigation of these conditions in MS composite CEs is in progress.

Funding statement

This work was supported by National Natural Science Foundation of China (Grant No. 21762033), Natural Science Foundation of Inner Mongolia (Grant No.2021MS02025 and 2021MS05047), the fundamental Research Funds for the Inner Mongolia Normal University (Grant No. 2023JBBJ006) and High-level overseas students Foundation of the Ministry of Human Resources and Social Security of China (2019).

Table 2
CV, EIS and Tefel polarization data of DSSCs based on the Pt, Pt/SBA-15 composite and SBA-15 CEs.

CE	J_{red} (mA/cm^2)	E_{pp} (V)	R_s (Ω cm^2)	R_{ct} (Ω cm^2)	J_{lim} (mA/cm^2)	J_0 (mA/cm^2)
Pt	−1.25	0.93	17.78	1.17	1.68	0.67
Pt/SBA1	−1.89	0.90	19.27	1.30	1.70	0.66
Pt/SBA2	−1.28	0.76	16.25	0.86	1.72	0.68
Pt/SBA3	−1.56	0.92	24.78	1.34	1.56	0.53
SBA-15	−0.79	0.98	21.84	3.35	0.71	−0.83

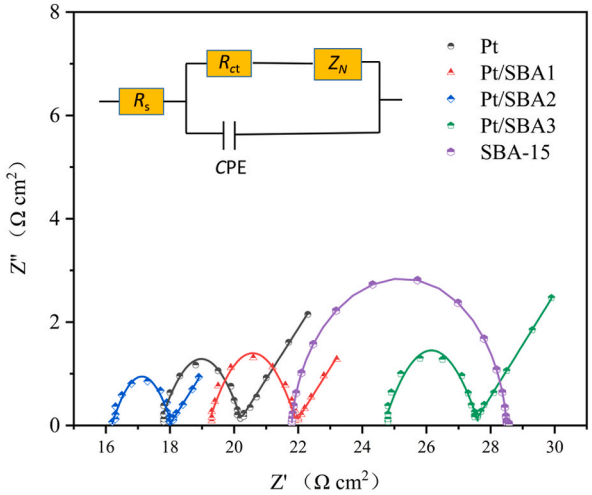

Fig. 6. Electrochemical impedance spectroscopy of Pt, Pt/SBA-15 composites and SBA-15 CEs, as well as the Randles-type equivalent circuit based on dummy cells.

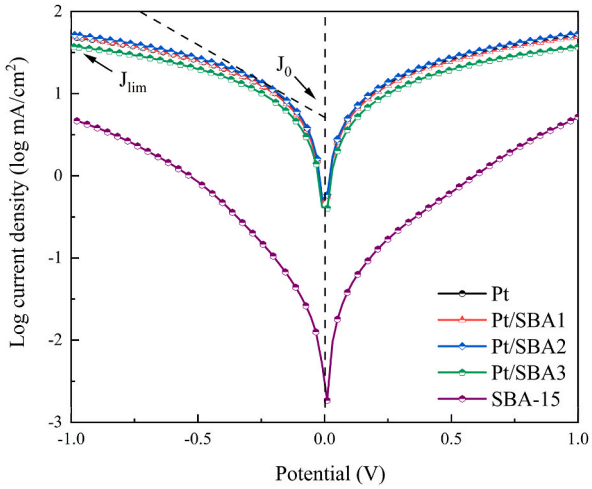

Fig. 7. Tafel polarization diagram of Pt, Pt/SBA-15 composites and SBA-15 CEs.

Data availability statement

Data will be made available on request.

Additional information

No additional information is available for this paper.

CRediT authorship contribution statement

Ding Nan: Software, Methodology, Investigation, Formal analysis, Data curation, Conceptualization. **Hongzhi Fan:** Software, Methodology, Investigation, Formal analysis, Data curation, Conceptualization. **Altan Bolag:** Writing – review & editing, Writing – original draft, Supervision, Resources, Project administration, Methodology, Investigation, Funding acquisition, Formal analysis, Data curation, Conceptualization. **Wenhui Liu:** Writing – original draft, Software, Data curation. **Tana Bao:** Resources, Funding acquisition.

Declaration of competing interest

The authors declare that they have no known competing financial interests or personal relationships that could have appeared to influence the work reported in this paper.

Appendix A. Supplementary data

Supplementary data to this article can be found online at https://doi.org/10.1016/j.heliyon.2023.e22403.

References

[1] J.V. Vaghasiya, K.K. Sonigara, L. Suresh, M. Panahandeh-Fard, S.S. Soni, S.C. Tan, Efficient power generating devices utilizing low intensity indoor lights via non-radiative energy transfer mechanism from organic ionic redox couples, Nano Energy 60 (2019) 457–466.
[2] B. O'Regan, M. Gratzel, A low-cost, high-efficiency solar cell based on dye-sensitized colloidal TiO_2 films, Nature 353 (1991) 737–740.
[3] M. Gratzel, Solar energy conversion by dye-sensitized photovoltaic cells, Inorg. Chem. Rev. 44 (2005) 6841–6851.
[4] A. Hagfeldt, G. Boschloo, L. Sun, L. Kloo, H. Pettersson, Dye-sensitized solar cells, Chem 110 (2010) 6595–6663.
[5] M. Freitag, J. Teuscher, Y. Saygili, X. Zhang, F. Giordano, P. Liska, J.L. Hua, S.M. Zakeeruddin, J.E. Moser, M. Gratzel, A. Hagfeldt, Dye-sensitized solar cells for efficient power generation under ambient lighting, Nat. Photonics 11 (2017) 372–378.
[6] S. Thomas, T.G. Deepak, G.S. Anjusree, T.A. Arun, S.V. Nair, A. Nair, A review on counter electrode materials in dye-sensitized solar cells, Chem. A. 2 (2014) 4474–4490.
[7] K. Saranya, Md Rameez, A. Subramania, Developments in conducting polymer based counter electrodes for dye-sensitized solar cells–An overview, Eur. Polym. J. 66 (2015) 207–227.
[8] K. Kumar, J. Kriz, N. Bennett, B.X. Chen, H. Upadhayaya, K.R. Reddy, V. Sadhu, Functionalized metal oxide nanoparticles for efficient dye-sensitized solar cells (DSSCs): a review, Mater. Sci. Energy Tech. 3 (2020) 472–481.
[9] S.S. Abdullaev, Y.F. Breesam, A.H. AlZubaidi, A.K. Tripathi, A.K. Kareem, S.V. Kuznetsov, T. Alawsi, R.S. Zabibah, ZnO@ZnCo2O4 core-shell: a novel high electrocatalytic nanostructure to replace platinum as the counter electrode in dye-sensitized solar cells, Mater. Sci. Semicond. Process. 165 (2023), 107709.
[10] K.A. Subalakshmi, Kumar, O.P. Paul, S. Saraswathy, A. Pandurangan, J. Senthilselvan, Platinum-free metal sulfide counter electrodes for DSSC applications: structural, electrochemical and power conversion efficiency analyses, Sol. Energy 193 (2019) 507–518.
[11] N. Kanjana, W. Maiaugree, T. Lunnoo, P. Laokul, I. Chaiya, A. Ruammaitree, P. Wongjom, Y. Infahsaeng, One-step hydrothermal synthesis and electrocatalytic properties of MoS_2/activated carbon composite derived from shallots, J. Appl. Electrochem. (2023) 1–10, https://doi.org/10.1007/s10800-023-01921-z.
[12] J.H. Wu, Z. Lan, J.M. Lin, M.L. Huang, Y.F. Huang, L.Q. Fan, G.G. Luo, Y. Lin, Y.M. Xie, Y.L. Wei, Counter electrodes in dye-sensitized solar cells, Chem. Soc. Rev. 46 (2017) 5975–6023.
[13] U.A. Kamarulzaman, M.Y.A. Rahman, M.S. Su'ait, A.A. Umar, Improvement of the performance of dye-sensitized solar cells employing NickelPalladium alloy-reduced graphene oxide counter electrode, Influence of palladium content, Optik 276 (2023), 170658.
[14] M. Aftabuzzaman, C.Y. Lu, H.K. Kim, Recent progress on nanostructured carbon-based counter/back electrodes for high-performance dye-sensitized and perovskite solar cells, Nanoscale 12 (2020) 17590–17684.
[15] M. Younas, N. Turki, Baroud, M.A. Gondal, M.A. Dastageer, P. Emmanuel, Giannelis, Highly efficient, cost-effective counter electrodes for dye-sensitized solar cells (DSSCs) augmented by highly mesoporous carbons, J. Power Sources 468 (2020), 228359.
[16] R.R. Francisco, The role of carbon materials in heterogeneous catalysis, Carbon 36 (1998) 159–175.
[17] E. Furimsky, Carbon materials for catalysis, Chem. Soc. 131 (2009) 9856–9857.
[18] M. Aftabuzzaman, C.Y. Lu, H.K. Kim, Recent progress on nanostructured carbon-based counter/back electrodes for high-performance dye-sensitized and perovskite solar cells, Nanoscale 12 (2020) 17590–17648.
[19] X.W. Li, R.X. Chen, L. Li, S.F. Wang, W.M. Zhang, K.Z. Wu, W.Y. Li, M.X. Wu, A comparative evaluation of catalytic activities of carbon molecular sieve counter electrode toward different redox couples in dye-sensitized solar cells, Electrochimi. Acta 200 (2016) 168–173.
[20] Q.P. Li, Y. Zhou, Preparation method, and biological application of mesoporous silica molecular sieves: a narrative review, Molecules 28 (2023) (2013).
[21] J.Q. Xu, H.L. Wang, F. Guo, C. Zhang, J.Q. Xie, Recent advances in supported molecular sieve catalysts with wide temperature range for selective catalytic reduction of NO_x with C_3H_6, RSC Adv. 9 (2019) 824–838.
[22] C. Martinez, A. Corma, Inorganic molecular sieves: preparation, modification and industrial application in catalytic processes, Coord. Chem. Rev. 255 (2011) 1558–1580.
[23] A. Bolag, Q. Wang, L. Liu, T. Jamiyansuren, U. Tumurpurev, N. Tuvjargal, T. Bao, J. Ning, H. Alata, O. Tegus, Improved photovoltaic performance of dye-sensitized solar cells using dual post treatment based on TiCl4 and urea solution, Micro & Nano Lett. 16 (2021) 232–238.
[24] Md M. Rahman, K. Inab, G. Batnyagt, M. Saikawa, Y. Kato, R. Awata, B. Delgertsetsega, Y. Kaneta, K. Higashi, T. Uruga, Y. Iwasawa, K. Uiab, T. Takeguchi, Synthesis of catalysts with fine platinum particles supported by high-surface-area activated carbons and optimization of their catalytic activities for polymer electrolyte fuel cells, RSC Adv. 11 (2021) 20601–20611.
[25] N. Sakai, S. Matile, Stack exchange strategies for the synthesis of covalent double-channel photosystems by self-organizing surface-initiated polymerization, J. Am. Chem. Soc. 133 (2011) 18542–18545.
[26] K.D. Zhang, S. Matile, Complex functional systems with three different types of dynamic covalent bonds, Angew. Chem. Int. Ed. 54 (2015) 1–5.
[27] D.F. Swinehart, J. Chem. Educ. 39 (1962) 333–335.
[28] T. Ahamad, $CoSe_2$@N-Doped graphene nanocomposite high-efficiency counter electrode for dye-sensitized solar cells, J. Inorg. Organomet. Polym. Mater. 32 (2022) 2568–2577.
[29] I.K. Popoola, M.A. Gondal, J.M. AlGhamdi, T.F. Qahtan, Photofabrication of highly transparent platinum counter electrodes at ambient temperature for bifacial dye sensitized solar cells, Sci. Rep. 8 (2018), 12864.

[30] N. Kanjana, W. Maiaugree, P. Laokul, I. Chaiya, T. Lunnoo, P. Wongjom, Y. Infahsaeng, B. Thongdang, V. Amornkitbamrung, Fly ash boosted electrocatalytic properties of PEDOT:PSS counter electrodes for the triiodide reduction in dye-sensitized solar cells, Sci. Rep. 13 (2023) 6012.
[31] N. Kanjana, S. Pimsopa, W. Maiaugree, P. Laokul, I. Chaiya, A. Chingsungnoen, P. Poolcharuansin, N. Ratchapolthavisin, W. Jarernboon, P. Wongjom, Novel micro-ceramic bottom ash mixed PEDOT:PSS/PVP for a low-cost Pt-free counter electrode in a dye sensitized solar cell, J. Electrochem. Soc. 169 (2022), 083503.
[32] A. Hauch, A. Georg, Diffusion in the electrolyte and charge-transfer reaction at the platinum electrode in dye-sensitized solar cells, Electrochim, Acta 46 (2002) 3457–3466.
[33] H. Sun, L. Zhang, Z.S. Wang, Single-crystal $CoSe_2$ nanorods as an efficient electrocatalyst for dye-sensitized solar cells, J. Mater. Chem. A 2 (2014), 16023.
[34] N. Kanjana, W. Maiaugree, S. Tontapha, P. Laokul, A. Chingsungnoen, S. Pimanpang, I. Chaiya, S. Daengsakul, V. Amornkitbamrung, Effect of carbonization temperature on the electrocatalytic property and efficiency of dye-sensitized solar cells derived from corncob and sugarcane leaf agricultural residues, Biomass. Convers. Bior 13 (2023) 8361–8371.
[35] W. Maiaugree, S. Lowpa, M. Towannang, P. Rutphonsan, A. Tangtrakarn, S. Pimanpang, P. Maiaugree, N. Ratchapolthavisin, W. Sang-aroon, W. Jarernboon, V. Amornkitbamrung, A dye sensitized solar cell using natural counter electrode and natural dye derived from mangosteen peel waste, Sci. Rep. 5 (2015), 15230.
[36] M. Younas, Turki N. Baroud, M.A. Gondal, M.A. Dastageer, Emmanuel P. Giannelis, Highly efficient, cost-effective counter electrodes for dye-sensitized solar cells (DSSCs) augmented by highly mesoporous carbons, J. Power Sources 468 (2020), 228359.